Measurement of the Muon-Decay Spectrum with a Wire Spark-Chamber Spectrometer*†

BRUCE ARNE SHERWOOD‡
Department of Physics
and
The Enrico Fermi Institute for Nuclear Studies, The University of Chicago, Chicago, Illinois
(Received 29 April 1966)

The momentum spectrum of muon-decay positrons has been investigated, in the region above 25 MeV, with a homogeneous magnet containing wire spark chambers with magnetic-core readout. At a given field, this spectrometer accepts, with essentially constant probability and a momentum resolution of $\pm 1\%$, a 30% momentum range. On the basis of 2.8×10^6 events we find for the Michel parameter the value $\rho=0.760\pm 0.009$ (in agreement with $V-A$) *provided* we constrain, as has been customary, the low-energy parameter η to be zero. Since the two-component neutrino hypothesis $(V+\epsilon A)$ predicts $\rho=\frac{3}{4}$ while leaving η free, it is more sensible to impose the constraint $\rho=\frac{3}{4}$ and fit for η; doing this, we obtain $\eta=-0.7\pm 0.6$, again in agreement with $V-A$, which predicts $\eta=0$.

WE have measured the electron spectrum in positive muon decay using a new technique.[1] The spectrometer consists of a homogeneous magnet containing wire spark chambers[2] with magnetic-core readout. In comparison with older techniques, this approach, while statistically powerful, offers improved control over systematic errors.

I. INTRODUCTION

A. Theory

Muon decay is important in testing weak-interaction theories because it is at present the only purely leptonic reaction experimentally accessible. Bouchiat and Michel[3] and Kinoshita and Sirlin[4] assumed an interaction Hamiltonian in muon decay of the form[5]

$$H=\sum_{i=1}^{5}(\bar{e}\Gamma_i\mu)(\bar{\nu}\Gamma_i(C_i+C_i'\nu_5)\nu)\,, \tag{1}$$

where $i=S,\ V,\ T,\ A,\ P$. This represents the most general local (derivative-free) interaction with lepton conservation[6] but without parity conservation. They calculated the electron momentum and angular distribution[7] to be

$$N(x,\hat{p})dxd\Omega=[M(x;\rho,\eta)-\xi\langle\boldsymbol{\sigma}_\mu\rangle\cdot\hat{p}B(x;\delta)]x^2dxd\Omega\,, \tag{2a}$$

where

$$M(x;\rho,\eta)=6(1-x)+\tfrac{4}{3}\rho(4x-3)+12\eta(m/m_\mu)[(1-x)/x]\,, \tag{2b}$$

$$B(x;\delta)=2(1-x)+\tfrac{4}{3}\delta(4x-3)\,, \tag{2c}$$

$$x=p/p_{\max}\,,\quad p_{\max}=52.827\ \mathrm{MeV}/c.$$

The parameters ρ, η, ξ, and δ are functions of the coupling constants:

$$\begin{aligned}
\rho&=\frac{3(\bar{V}^2+A^2)+6\bar{T}^2}{(\bar{S}^2+\bar{P}^2)+4(\bar{V}+\bar{A}^2)+6T^2}\,,\\
\eta&=\frac{(\bar{S}^2-\bar{P}^2)+2(\bar{A}^2-\bar{V}^2)}{(\bar{S}^2+\bar{P}^2)+4(\bar{V}^2+\bar{A}^2)+6\bar{T}^2}\,,\\
\xi&=\frac{2\,\mathrm{Re}[3(SP'^*+S'P^*)-4(VA'^*+V'A^*)-14TT'^*]}{(\bar{S}^2+\bar{P}^2)+4(\bar{V}^2+\bar{A}^2)+6\bar{T}^2}\,,\\
\delta&=\frac{\mathrm{Re}[-3(VA'^*+V'A^*)-6TT'^*]}{\mathrm{Re}[3(SP'^*+S'P^*)-4(VA'^*+V'A^*)-14TT'^*]}\,,
\end{aligned} \tag{3}$$

where $S=C_1$, $S'=C_1'$, $\bar{S}^2=|S|^2+|S'|^2$, etc.[8] Much earlier, Michel[9] had obtained $M(x;\rho,\eta)$ assuming parity conservation.

The terms involving the shape parameters ρ and δ vanish when integrated over the whole spectrum, so that the angular distribution of the integrated spectrum is given by $1+\bar{a}\cos\theta$, where the integrated asymmetry $\bar{a}$ is given by $\bar{a}=\xi/3$ if the small η term is neglected.

* Research supported by the U. S. Office of Naval Research.
† A thesis submitted to the Department of Physics, The University of Chicago, in partial fulfillment of the requirements for the Ph.D. Degree.
‡ Woodrow Wilson Fellow, 1961–1962; National Science Foundation Fellow, 1962–1965. Present address: Department of Physics, California Institute of Technology, Pasadena, California.
[1] B. A. Sherwood, R. D. Ehrlich, D. Fryberger, R. J. Powers, V. L. Telegdi, and J. Bounin, paper presented at the American Physical Society Meeting in New York, January 1965 (unpublished); IEEE Trans. Nucl. Sci. **12**, 49 (1965).
[2] M. J. Neumann and H. Sherrard, IEEE Trans. Nucl. Sci. **9**, 259 (1962); **9**, 58 (1962). For other references, see W. A. Higinbothan, *ibid.* **12**, 199 (1965).
[3] C. Bouchiat and L. Michel, Phys. Rev. **106**, 170 (1957).
[4] T. Kinoshita and A. Sirlin, Phys. Rev. **107**, 593 (1957).
[5] We will not concern ourselves with problems relating to the nonidentity of the electron and muon neutrinos.
[6] For a more general discussion in terms of the Pauli-Pursey invariants, including lepton nonconservation, see R. Gatto and G. Lüders, Nuovo Cimento **7**, 806 (1958).
[7] This is correct for μ^- decay. The result for μ^+ decay is obtained by $\xi\to-\xi$. We shall omit the normalization since we are interested only in the spectral shape. Unless stated otherwise, "electron" means a positive or a negative electron.
[8] ξ and δ are as defined in Ref. 4. There seems to be a slight disagreement with the definitions of the related parameters α and β of Ref. 3.
[9] L. Michel, Proc. Phys. Soc. (London) **A63**, 514 (1950).

Because the observables associated with the two neutrinos are in practice inaccessible, the ten (possibly complex) coupling constants of Eq. (1) are experimentally underdetermined. Only six (real) quantities can be measured: τ, ρ, η, ξ, δ, and the electron helicity.[10]

The two-component neutrino hypothesis[11] restricts the interaction to V and A, with $V'=+V$, $A'=+A$ (if the neutrino is left-handed), and the expressions for ρ, η, ξ, and δ reduce to

$$\rho=\tfrac{3}{4};\quad \eta=-\tfrac{1}{2}\left(\frac{|V|^2-|A|^2}{|V|^2+|A|^2}\right);$$
$$\xi=\frac{-2\,\mathrm{Re}(VA^*)}{|V|^2+|A|^2};\quad \delta=\tfrac{3}{4}. \tag{4}$$

In this case measurements of ρ and δ cannot furnish any information concerning the relative magnitude (and phase) of the V and A couplings.

If the further assumption is made[12] that not only the neutrino but *all* leptons are left-handed (i.e., their fields appear in the interaction in association with $[1+\gamma_5]$), then we have the "$V-A$" theory, and

$$\rho=\tfrac{3}{4};\quad \eta=0;\quad \xi=1;\quad \delta=\tfrac{3}{4}. \tag{5}$$

The only free parameter left is the coupling constant V (equivalently, A) which determines the lifetime.

The results above are modified by corrections arising from the electromagnetic interactions (real and virtual) of the charged leptons. These have been calculated[13] for the two-component theory (which fixes ρ and δ), yielding a spectrum of the form

$$\left\{\left[3-2x+\left(\frac{\alpha}{2\pi}\right)f(x)+12\eta\frac{m_e}{m_\mu}\left(\frac{1-x}{x}\right)\right]\right.$$
$$\left.+\xi\langle\boldsymbol{\sigma}_\mu\rangle\cdot\hat{p}_e\left[1-2x+\left(\frac{\alpha}{2\pi}\right)h(x)\right]\right\}x^2dxd\Omega\,, \tag{6}$$

where α is the fine-structure constant. If terms of order m_e/m_μ are neglected, the radiative corrections are the same for V and for A,[14] so that to this order the functions $f(x)$ and $h(x)$ apply to a two-component theory with arbitrary V/A.

If the true coupling is anticipated to be very nearly that given by the two-component theory, then it is useful to compare the experimental spectrum with an expression of the form

$$\left\{\left[1+\frac{(\alpha/2\pi)f(x)}{3-2x+12\eta(m_e/m_\mu)(1-x)/x}\right]M(x;\rho,\eta)\right.$$
$$\left.-\xi\langle\boldsymbol{\sigma}_\mu\rangle\cdot\hat{p}\left[1+\frac{(\alpha/2\pi)h(x)}{1-2x}\right]B(x;\delta)\right\}x^2dxd\Omega\,, \tag{7}$$

which reduces to Eq. (6) in the two-component case.

It is well known[15] that the local interaction given by Eq. (1) cannot be entirely correct, since at very high energies (several hundred BeV) unitarity would be violated. If the weak interaction were mediated by a boson W of mass M_W, then terms of order $(M_\mu/M_W)^2$ would arise in the spectrum. However, attempts to produce W's in neutrino reactions have so far failed, leading to a limit on the W mass of $M_W\geqslant 2$ BeV,[16] in which case no experiment on muon decay to date including the present one would be likely to see effects of the W. For example, $M_W=2$ BeV leads to a modification of ρ by about 0.001, whereas the smallest quoted error in ρ is 0.003.[17]

B. Experimental History

Over the past decade many measurements of the muon-decay spectrum have been performed, primarily with emphasis on the determination of the parameter ρ.[17–24] In general, their results were consistent with $\rho=\frac{3}{4}$,

[10] For a general discussion see T. Kinoshita and A. Sirlin, Phys. Rev. **108**, 844 (1957). They show that if electrons of a specified handedness are selected, additional parameters become available for measurement; however, such a selection appears experimentally impractical, and furthermore the coupling constants remain underdetermined.

[11] T. D. Lee and C. N. Yang, Phys. Rev. **105**, 1671 (1957); A. Salam, Nuovo Cimento **5**, 299 (1957); L. Landau, Nucl. Phys. **3**, 127 (1957).

[12] E. C. G. Sudarshan and R. E. Marshak, Phys. Rev. **109**, 1860 (1958); R. P. Feynman and M. Gell-Mann, *ibid.* **109**, 193 (1958).

[13] T. Kinoshita and A. Sirlin, Phys. Rev. **113**, 1652 (1959); S. M. Berman, *ibid.* **112**, 267 (1958).

[14] For a discussion, see A. Sirlin, in *Lecture Notes on Weak Interactions and Topics in Dispersion Physics from the Second Bergen International School of Physics*, edited by Christian Fronsdal (W. A. Benjamin, Inc., New York, 1963).

[15] T. D. Lee and C. N. Yang, Phys. Rev. **128**, 885 (1962); T. D. Lee, *ibid.* **128**, 899 (1962).

[16] M. M. Block, H. Burmeister, D. C. Cundy, B. Eiben, C. Franzinetti, J. Keren, R. Møllerud, G. Myatt, M. Nikolic, A. Orkin-Lecourtois, M. Paty, D. H. Perkins, C. A. Ramm, K. Schultze, H. Sletten, K. Soop, R. Stump, W. Venus, and H. Yoshiki, Phys. Letters **12**, 281 (1964); G. Bernardini, J. K. Bienlein, G. Von Dardel, H. Faissner, F. Ferrero, J. M. Gaillard, H. J. Gerber, B. Hahn, V. Kaftanov, F. Kreinen, C. Manfredotti, M. Reinharz, and R. A. Salmeron, *ibid.* **13**, 86 (1964); R. Burns, K. Goulianos, E. Hyman, L. Lederman, W. Lee, N. Mistry, J. Rettberg, M. Schwartz, J. Sunderland, and G. Danby, Phys. Rev. Letters **15**, 42 (1965). The search for W production in nucleon-nucleon reactions has yielded similar lower limits on the W mass: R. C. Lamb, R. A. Lundy, T. B. Novey, D. D. Yovanovitch, M. L. Good, R. Hartung, M. W. Peters, and A. Subramanian, *ibid.* **15**, 800 (1965); R. Burns, G. Danby, E. Hyman, L. M. Lederman, W. Lee, J. Rettberg, and J. Sunderland, *ibid.* **15**, 830 (1965).

[17] M. Bardon, P. Norton, J. Peoples, A. M. Sachs, and J. Lee-Franzini, Phys. Rev. Letters **14**, 449 (1965); see also J. Peoples, Nevis Report No. 147, 1966 (unpublished).

[18] H. Kruger, University of California Radiation Laboratory Report No. UCRL 9322, 1961 (unpublished).

[19] L. Rosenson, Phys. Rev. **109**, 958 (1958).

[20] W. F. Dudziak, R. Sagane, and J. Vedder, Phys. Rev. **114**, 336 (1959).

[21] R. J. Plano, Phys. Rev. **119**, 1400 (1960).

[22] M. Block, E. Fiorini, E. Kikuchi, G. Giacomelli and S. Ratti, Nuovo Cimento **23**, 1114 (1962).

[23] J. Barlow, P. S. L. Booth, L. J. Carroll, G. R. Court, J. D. Davies, D. N. Edwards, R. G. Johnson, and J. R. Womald, Proc. Phys. Soc. (London) **84**, 239 (1964).

[24] D. B. Pontecorvo and R. M. Sulyaev, in *Proceedings of the 12th Annual International Conference on High-Energy Physics, Dubna, 1964* (Atomizdat, Moscow, 1965).

though there are some striking exceptions (see Table I). Magnetic spectrometers, while capable of high statistics, appear to be subject to systematic errors brought about primarily by scattering and degradation of high-energy electrons in slits and walls. On the other hand, bubble chambers, though relatively free of systematic errors, seem to be severely limited by statistics. The advent of filmless spark-chamber techniques opened the way to the construction of spectrometers which retain the advantages of these two techniques without having their limitations.

A spectrometer consisting of low-mass spark chambers placed in a homogeneous magnetic field is capable of high momentum resolution, can determine the entire electron trajectories in such a way as to eliminate wall-scattering events, and can handle large volumes of data, in particular in conjunction with a computer. A Columbia group[25] built such a system using acoustic spark chambers, whereas we adopted the digitized wire spark chambers as developed in the Institute for Computer Research of this university.[2]

We set as our first goal the measurement of the parameter ρ to better than ± 0.01. Further, we wanted to measure the parameter δ in a subsequent experiment with essentially the same spectrometer.

The spectrometer was designed to measure the high-energy region of the spectrum, because ρ has its greatest effect there. In predicting the number of events required for a given statistical error in ρ we neglected the numerically small (m/m_μ) term involving η. Only after completing the experiment did we realize that including η in the analysis has, even at high energies, a drastic effect.[26] For N events falling in the energy region $0.75 \leqslant x \leqslant 1$, the standard deviation in ρ is $2.6/\sqrt{N}$, *if* the η term is neglected (i.e., η *constrained* to be zero). On the other hand, if a simultaneous fit for ρ and η is made, the standard deviation in ρ increases to $30/\sqrt{N}$; the standard deviation in η is $3000/\sqrt{N}$. From Eq. (3) it is seen that $|\eta| \leqslant 1$. Imposing this constraint on η, the error in ρ becomes approximately $2.6/\sqrt{N}+0.01$ (unless N is so large, $\sim 10^7$, that $|\eta|$ is determined to better than its maximum value). The reason for this is that a large but reasonable $\eta(|\eta| \leqslant 1)$ affects the spectrum in a way comparable to what a small *change* in ρ would do. An experiment in which the *entire* spectrum $(0 \leqslant x \leqslant 1)$ is determined is statistically far more advantageous; then the ρ-η correlation is much reduced, because the difference in the ρ- and η-associated functional forms emerges clearly.

Plano[21] appears to have been the only experimenter who included the effect of η in his analysis.[27] With η constrained to $\eta=0$, Plano obtained $\rho=0.780\pm0.016$; from a simultaneous fit for ρ and η he obtained $\rho=0.745 \pm 0.025$ and $\eta=-2.0\pm0.9$ (statistical errors only). This value of η was dismissed by Plano as being related to an apparent deficiency of low-energy electrons.[28]

TABLE I. Experimental values of ρ.

Method	ρ	Institution	
Diffusion chamber	0.67 ± 0.05	Chicago[a]	(1958)
Spiral orbit spectrometer	0.741 ± 0.027	LRL[b]	(1959)
H_2 bubble chamber	0.780 ± 0.025	Columbia[c]	(1960)
Magnetic spectrometer	0.774 ± 0.042	LRL[d]	(1961)
He bubble chamber (μ^-)	0.751 ± 0.034	Duke[e]	(1962)
Magnetic spectrometer	0.661 ± 0.016	Liverpool[f]	(1964)
Diffusion chamber (μ^-)	0.867 ± 0.035	Dubna[g]	(1964)
Sonic spark-chamber spm.	0.750 ± 0.003	Columbia[h]	(1965)
Wire spark-chamber spm.	0.760 ± 0.009	Chicago[i]	(1965)

[a] L. Rosenson, Ref. 19.
[b] W. F. Dudziak *et al.*, Ref. 20.
[c] R. J. Plano, Ref. 21.
[d] H. Kruger, Ref. 18.
[e] M. Block *et al.*, Ref. 22.
[f] J. Barlow *et al.*, Ref. 23.
[g] D. B. Pontecorvo *et al.*, Ref. 24.
[h] M. Bardon *et al.*, Ref. 17.
[i] This experiment.

All other experimenters constrained η to $\eta=0$ and fit for ρ alone, so that their quoted errors on ρ are to be increased by varying amounts, depending on the ρ-η correlation obtaining for the momentum range measured. For the more accurate measurements the error on ρ is not set by statistics but by the constraint $|\eta| \leqslant 1$, the only general constraint.[29] Plano imposed the constraint[30] $\eta^2 \leqslant (1-\xi^2)/4$ to restrict η further and thus reduce the ρ-η correlation; this is, however, illegitimate, as this inequality holds *only* under the two-component neutrino hypothesis (the equality sign holding for V and A relatively real), which *constrains* ρ to $\rho=\frac{3}{4}$. If interactions more general than $V+\epsilon A$ are to be considered, it is necessary to fit for ρ and η simultaneously; otherwise, if $V+\epsilon A$ is assumed, the only consistent procedure is to constrain ρ to $\frac{3}{4}$ and fit for η alone.

If the two-component neutrino hypothesis is correct, then the measurement by Gurevich *et al.*[31] of the integrated asymmetry $a=0.325\pm0.010$ (which implies $\xi=0.978\pm0.030$, including radiative corrections) constrains η to $|\eta| \leqslant 0.11_{-0.11}^{+0.06}$, the equality holding for V and A relatively real. If the two-component hy-

[25] M. Bardon, J. Lee, J. Peoples, A. M. Sachs, and G. Sutter, Bull. Am. Phys. Soc. **8**, 389 (1963); M. Bardon, J. Lee, P. Norton, J. Peoples, and A. M. Sachs, CERN Report No. 64-30, p. 41 (unpublished).

[26] Unfortunately the remark of Dudziak *et al.* (Ref. 20), footnote 17, escaped our attention.

[27] After the original version of this article was written, there came to our attention the thesis of Peoples (Ref. 17), in which certain particular assumptions are made in order to place stringent restrictions on η and to minimize the ρ-η correlation. We will not follow this approach here.

[28] This may be due to applying a correction for external bremsstrahlung which, in our opinion, is too large. It might further be that the radiative corrections at low energies are inaccurate, due to neglect of the electron mass.

[29] An inequality involving ρ and η was given by L. Michel, thesis, Universite de Paris, 1953 (unpublished). This inequality is apparently invalid when inner bremsstrahlung is taken into account.

[30] T. Kinoshita and A. Sirlin, Phys. Rev. **107**, 593 (1957). The factor $\frac{1}{4}$ (which was erroneously omitted by Plano) results from their definition of the low-energy parameter as 2η.

[31] I. I. Gurevich, L. A. Makariyna, B. A. Nikol'sky, B. V. Sokolov, L. V. Surkova, S. Kh. Khakimov, V. D. Shestakov, Yu. P. Dobretsov, and V. V. Akhmanov, Phys. Letters **11**, 185 (1964).

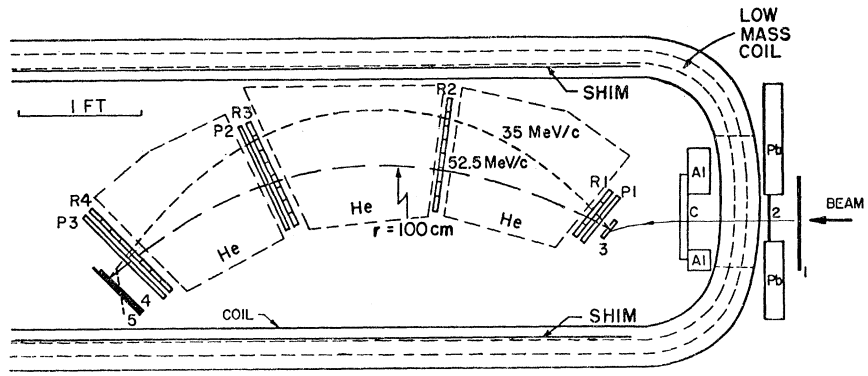

FIG. 1. Experimental arrangement. $R1$ through $R4$ and $P1$ through $P3$ are wire spark chambers. The magnet is totally enclosed, and provides over most of the region of interest a field homogeneous to $<0.05\%$. He-filled boxes (shown dashed) with 5×10^{-4}-in. Mylar windows are placed between the chambers to reduce multiple scattering.

pothesis is not assumed, the measurements to date of the observables in muon decay do not rule out rather large admixtures of S, T, and P.[32]

In order to compare our results with previous experiments, in what follows we will often refer to the measurement of ρ, neglecting η, but the final results will take the above discussion into consideration.

II. APPARATUS AND DATA RATES

A full description of the design and construction of the wire-chamber spectrometer is given in Appendix A. Fig. 1 shows the layout of the seven chambers in a homogeneous magnetic field; four chambers ($R1$–$R4$) measure the radius and three chambers ($P1$–$P3$) measure the pitch of the helical trajectory of the μ-decay electron. (The construction and performance of these wire spark chambers are discussed in Appendix B.) Counters 1 and 2 define the incoming positive-pion beam, counter 3 detects the π-μ decay, and counters 3, 4, and 5 detect the μ-decay positron.

Figure 2 shows the electronics for trigger selection. Pulses from a dynode of the photomultiplier of counter 3 fire a tunnel diode discriminator; two discriminator pulses, separated by more than 7 nsec and less than 70 nsec, signal a π-μ decay in the counter, generating an output from the "μ" gate. This circuit[33] was tested extensively in good stops geometry, and there were 0.4 "μ's" per stopping pion, the loss being explained by early decays, pion stops in scintillator wrappings, and muon escape. An "e" coincidence is generated by a $345\bar{1}\bar{2}$ signature, where the pulse from 3 is taken from the photomultiplier anode and amplified by a gain of 10. The "e" output is sent to two gates opened by a prompt and delayed "μ" signal. A "μ" followed by an "e" in the interval $0.1<t<5.1$ μsec is "real" and an "e" in the interval $17<t<22$ μsec is "accidental." Both the "real" and "accidental" outputs are used to fire the spark chambers and initiate readout, and they also set flip-flops which label the event, making it possible to perform a reliable background subtraction.

Part of the data was collected on line with the computer MANIAC III and part was collected with an incremental magnetic tape[34] recorder. In the latter mode we ran at reduced beam rates to minimize losses due to the $\sim$0.3-sec dead time needed for recording an event; the reduced rate also cut down on spurious sparks in the chambers. At the reduced rate, we had typically 220×10^3 (12)/sec, 12×10^3 (123)/sec, 1×10^3 (μ)/sec, 40 ($345\bar{1}\bar{2}$)/sec, and 1.4 (wire-chamber triggers)/sec. At 1734 G we collected 1450×10^3 triggers (950×10^3 on tape and 500×10^3 on line), and at 1300 G we collected 580×10^3 triggers.

Data collected on line were analyzed with an ALGOL program. Data on magnetic tape were analyzed on an IBM 7094; a FAP subroutine determined spark centroids from the 32-bit parallel input data, and the rest of the analysis was performed with a FORTRAN II program. Complete analysis, including geometrical reconstruction and selection according to various criteria, required approximately 10 msec per event.

III. EVENT-SELECTION CRITERIA

It is imperative that the criteria by which events are selected as "acceptable" either introduce no momentum bias or at least depend on momentum in a known way. In this section we shall examine the selection criteria that we adopted, and discuss the potential sources of bias.

The muons should be unpolarized for the measurement of the isotropic spectrum. Although the muon sample is produced in the target counter by stopping pions, it could in principle still have some slight net polarization. This could come about by a nonuniform pion stop distribution through the depth of that counter and by particular "π" and "μ" pulse-height requirements in triggering. However, the rapid rate of muon precession over a long (5-μsec) time range of observation effectively depolarizes the sample; even fully polarized muons would have an effective polarization of less than

[32] Cecilia Jarlskog, Nucl. Phys. **75**, 659 (1966). See also V. L. Telegdi, in Proceedings of the Argonne International Conference on Weak Interactions, 1965 (to be published).

[33] This important circuit was suggested by Professor V. L. Telegdi; the design was carried out by T. A. Nunamaker.

[34] Honeywell Model 6200.

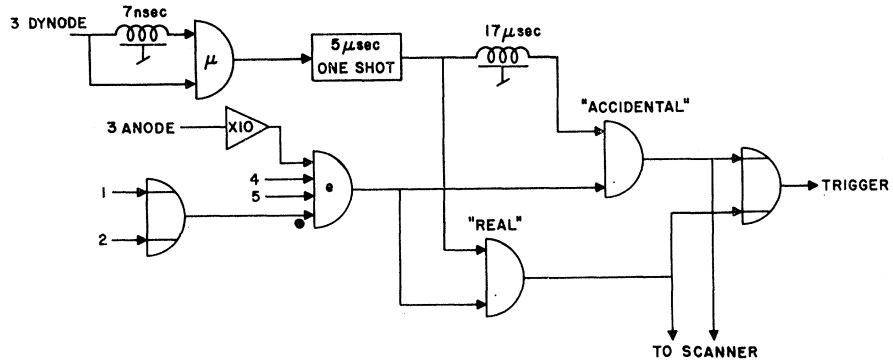

FIG. 2. Electronic logic for triggering the wire spark chambers and for labeling the event as "real" or "accidental."

0.5%. In addition, the target material (scintillator plastic) depolarizes muons.[35] Polarization is hence not considered a source of bias.

The electrons emerging from the source counter produce pulses of heights proportional to their collisional energy loss; this loss is practically momentum-independent over the momentum range of interest. Therefore, including this pulse in the trigger logic does not lead to a momentum bias.

Occasionally, a positron emerging from the target counter will be accompanied by a delta ray which may also register in the first chamber, in which case we do not analyze the event. For delta rays of momentum sufficient to avoid being bent away from the first chamber by the field ($p \gtrsim 0.5$ MeV/c), the probability of emission is only 3% and is, moreover, independent of the initial positron momentum.

The probability of annihilation in flight of the decay positions in counter 3, counter 4, and part of counter 5 (~ 1 g/cm^2 in all), is inversely proportional to the momentum and equal to 0.3% at 50 MeV/c. A small correction was applied.

Making reference to Fig. 3, we shall next discuss the momentum dependence $\Delta\Omega(p)$ of the solid angle $\Delta\Omega$ subtended at the source by the final-electron counter, or by a virtual detector plane effectively drawn in the data-analysis computer program.

If a point source A is located on the perpendicular bisector of a surface BC (of height h out of the plane of the drawing) and is connected by circular arcs of equal radius r to the points B and C, then the circular segments whose chords are AB and AC are congruent; hence $\Phi = \angle DAE = \angle CAB$. This result is independent of the radius r, as long as $r > a = \frac{1}{2}AB$. The arc lengths AB, AC are given by $2r \arcsin(a/r)$, and for $\Phi \ll 1$ and $h/a \ll 1$ the solid angle subtended at A by the plane surface BC is

$$\Delta\Omega(r) = (h\Phi/2a)[(r/a)\arcsin(a/r)]^{-1}. \quad (8)$$

In our spectrometer $1.33 \leqslant a/r \leqslant 1.78$, so that $1.07 \leqslant [(r/a)\arcsin(a/r)]^{-1} \leqslant 1.13$. This small (6%) variation in $\Delta\Omega$ can be further reduced by turning the surface BC through an angle α as indicated in Fig. 3. The dependence of $\Delta\Omega$ on r then becomes

$$\Delta\Omega(r) = (h\Phi/2a)[(r/a)\arcsin(a/r)]^{-1} \times \{1 + \tan\alpha[(r/a)^2 - 1]^{-1/2}\} \quad (9)$$

to order Φ^3. Numerical evaluation of (8) shows that, for $\alpha = 8°$, $\Delta\Omega(r)$ varies only by 0.1% within the given range of x. This was checked by calculating the solid angle by numerical integration; the results of the two methods were in agreement.

Since $\Delta\Omega(r)$ is computed, it might seem that a flat momentum acceptance has no special virtue. This conclusion is, however, incorrect, in view of the effect of a finite source. When $\Delta\Omega$ is considered as a function not only of r, but also of the source-point location (x_s, y_s), one finds that $\partial\Delta\Omega(r, x_s, y_s)/\partial x_s$ and $\partial\Delta\Omega(r, x_s, y_s)/y_s$ are minima when $\Delta\Omega(r)$ is flat. Thus an arrangement as sketched in Fig. 3 helps to minimize effects due to nonuniform source illumination and due to uncertainties in locating the source counter with reference to the wire chambers. One can, of course, deduce from the data both the muon illumination of the source counter and the electron illumination of the virtual detector, and use this information to check and to correct the theoretical solid angle $\Delta\Omega(p)$.

An alternative, more traditional, approach to the

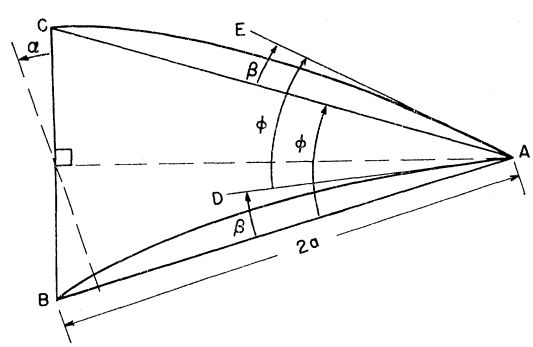

FIG. 3. Geometrical construction for deriving the solid angle $\Delta\Omega(r)$ in a magnetic field.

[35] R. A. Swanson, Phys. Rev. **112**, 580 (1958). See, however, G. Charpak, F. J. M. Farley, R. L. Garwin, T. Muller, J. C. Sens, V. L. Telegdi, C. M. York, and A. Zichichi, Nuovo Cimento **22**, 199 (1961).

solid-angle problem is to impose on the electrons the requirement that their momenta at emergence from the source lie within a given solid angle. The orientation of such a solid angle is then a function of momentum and point of origin in the source, unless the overlapping part of all these solid angles is used. In that case the total solid angle is much smaller than need be. Imposing the solid-angle requirement at the end of the trajectory rather than at the beginning allows one to retain many more of the events for analysis.

The final counters 4 and 5 were placed parallel to the final wire chamber to minimize the lever arm for outscattering from that chamber. Since the wire chambers were placed essentially perpendicular to the electron trajectories, the final counters were physically turned through $\alpha \approx 45°$ rather than $\alpha = 8°$. Thus the over-all wire-chamber trigger required the traversal of the physical counter, whereas the analysis program imposed the traversal of a "virtual" detector, oriented with $\alpha = 8°$. The size and location of this virtual detector were such that all trajectories which traversed it had also to traverse the physical counter.

The illuminations of the source counter and of the "virtual" electron detector were obtained from the data. The virtual detector was found to be uniformly illuminated at all momenta, which checks our solid-angle calculations and also shows that the spark chambers were uniformly efficient across their widths (as had been established in prior studies outside the magnet), a necessary condition for lack of momentum bias. The illumination of the source counter was not uniform (due to the uneven distribution of the incoming pion beam), but it was such that the net solid angle $\Omega(p)$ was essentially unchanged from that calculated for a point source.

Of the spark-chamber triggers, about a third were caused by electrons which missed the active volume of the spectrometer, as evidenced by simultaneous misses in adjacent chambers ($R3$ and $P2$, $R4$ and $P7$). These were presumably due to electrons which scattered off the magnet walls or other material. About 10% of the triggers had extra (spurious) sparks, due mainly to beam particles hitting chambers $R1$, $R2$, and $P1$. The rest of the triggers had one and only one spark in each of the seven chambers, and these events were retained for full analysis.

A trial circle radius was determined from the spark locations in $R1$, $R2$, $R3$, and this circle was extrapolated to $R4$. The deviation Δ_4 of the actual spark location in $R4$ from the extrapolated location was used to correct the trial momentum by an amount $\Delta p'$, and distributions of the deviations Δ_4 and $\Delta p'$ were collected. The pitch of the helical trajectory was determined from the spark locations in $P1$ and $P2$, and the distribution of the deviations Δ_z of the spark location in $P3$ from the locations predicted by extrapolation from $P1$ and $P2$ was also collected. (The pitch was not corrected using Δ_z, since the maximum pitch angle of 0.2 rad contributed only 0.04 to the final momentum.) The Δ_4 and Δ_z distributions are shown in Fig. 4, and the $\Delta p'$ distribution is shown in Fig. 5. The total momentum p of each event was then obtained from the momentum perpendicular to the field and the pitch. An event was considered "good" if $|\Delta p'| < 0.04$ (all momenta are measured in natural units, i.e., in units of $\frac{1}{2}m_\mu c = 53.827$ MeV/c) and $|\Delta_z| < 2.5$ cm. For such events the helices

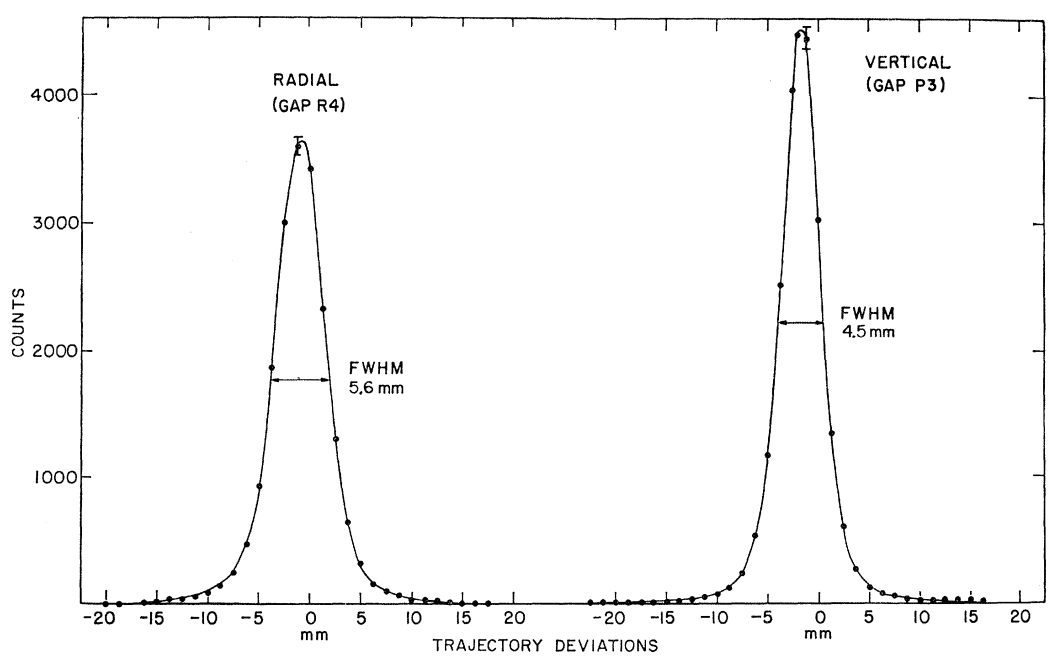

FIG. 4. Distributions of the radial and pitch deviations Δ_4 and Δ_z.

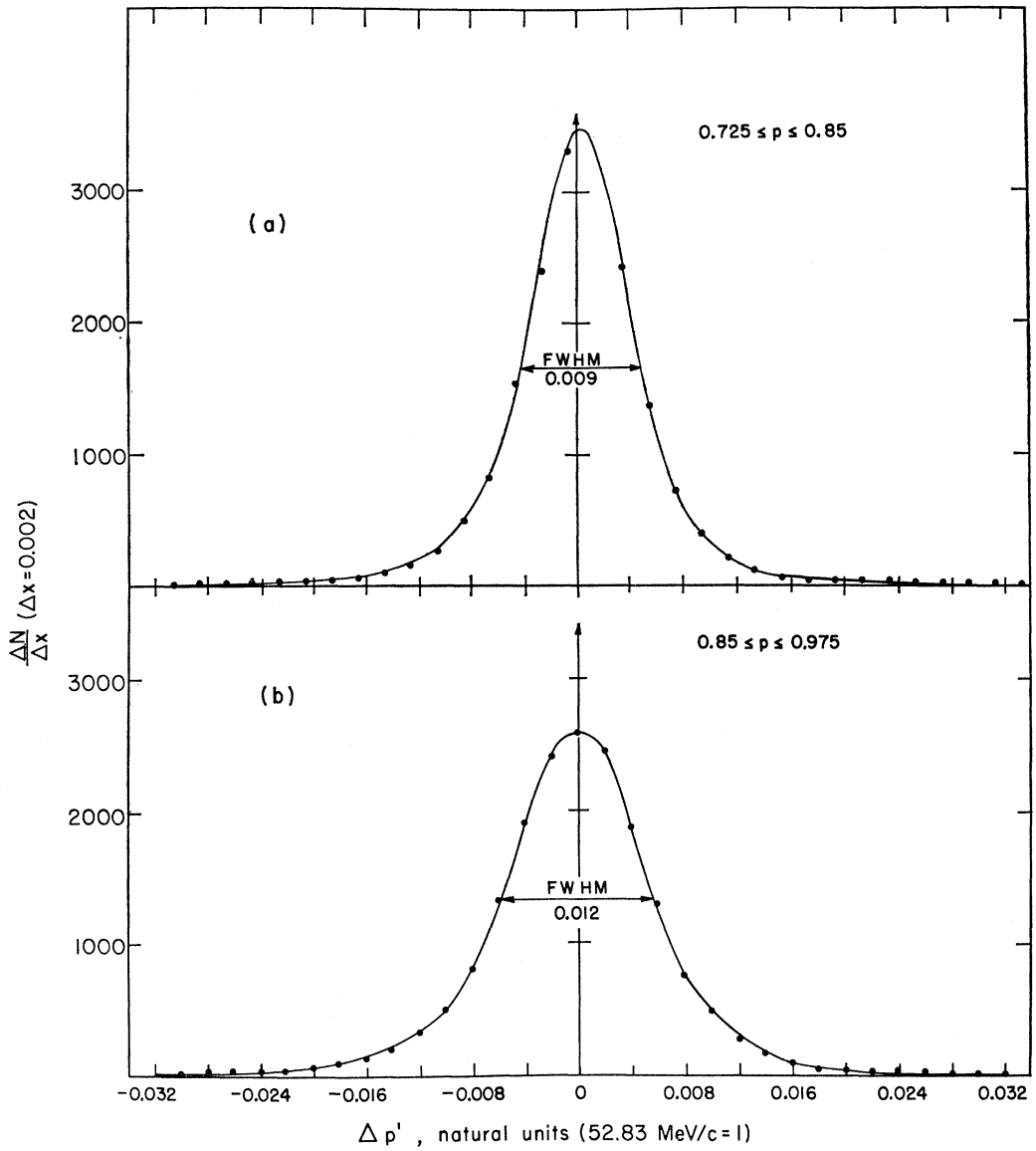

FIG. 5. Distribution of $\Delta p'$, the difference between the trial and fitted momenta (p_T and p). This distribution is narrower than the intrinsic resolution of the spectrometer, because p_T and p are correlated.

were extrapolated to check whether they came from the source counter and traversed the final virtual counter. Events were then assigned to the "real" or accidental spectrum.

Neglecting the pitch as a small correction, the quantity $\Delta p'$ is the difference between the trial momentum p_T and the final measured momentum p. The $\Delta p'$ distribution is closely related to the response of the spectrometer to a monoenergetic, massless source. The $\Delta p'$ distribution is, however, narrower than the true response function because there exists a positive correlation between the trial and final measured momenta.

It is important to establish whether the $\Delta p'$ and Δ_z selection criteria imposed are momentum dependent, and, if they are, to what extent. Inspection of the $\Delta p'$ distribution (Fig. 5) reveals that it is not truly Gaussian: Its shape is rather that of a Gaussian with "wings." However, its fractional area outside $|\Delta p'| < 0.04$ (the cutoff imposed) but within $|\Delta p'| < 0.08$ is only 0.5%, and is furthermore independent of momentum. It therefore appears reasonable that our $\Delta p'$ selection criterion does not lead to any significant momentum bias. A similar situation holds for Δ_z.

Note that the layout of the spectrometer is such that the characteristics of the trajectories (sagittae, arc lengths, bending angles) change little over a 30% momentum interval. This is borne out by the Δ_4, Δ_z, and $\Delta p'/p$ distributions, whose widths change by only $\approx 25\%$ across this interval. In particular, the effect of multiple scattering is nearly constant, since the increase

in multiple scattering with decreasing momentum is offset by an increase in bending angle. The variation of the percentage resolution with momentum is due mainly to the fact that the sagittae, which shrink with increasing momentum, are determined with a constant spatial resolution.

A. Background

The only significant background was contributed by decay electrons originating outside the source counter; such electrons may distort the spectrum due to geometrical bias. This background was minimized by placing the source far from the magnet walls and shielding from the beam that region of the magnet from which electrons could traverse counters 3, 4, and 5. In addition, such electrons could trigger the system only by making an accidental coincidence with the "μ" gate, so that they were removed by the simultaneous background subtraction made possible by the "real" and "accidental" labels generated by the logic shown in Fig. 2 and described in Sec. II.

For half of the 1734-G data the shape of the "accidental" spectrum was the same as that of the "real" spectrum, and the "accidentals" were 2% of the "reals." These accidentals were due to prompt, unobserved π-μ decays in the source and hence exhibited no momentum bias.

Half of the 1734-G data (and all of the 1300-G data) was collected without immediate analysis, due to circumstances beyond our control. As soon as it was analyzed, the "accidental" spectrum was found to vary between 3 and 10% of the "real" spectrum as a function of momentum. This momentum dependence was traced to muon decays in parts of the moderator located inside the magnet. It was eliminated by placing that moderator in a manner that electrons originating therein could not trigger the system.

We established that the real and accidental gates had equal widths by measuring them on an oscilloscope, and also by sending random pulses through them. In addition, the values of ρ obtained from the spectra with "high" and with "low" accidentals agree within statistics and have similar χ^2's. Furthermore, the 1300-G data also exhibit a good fit.

Backgrounds due to beam particles were essentially absent. The "μ" requirement and the 100-nsec delay in the "μ" gate ensured that a traversing pion or muon could trigger the system only accidentally. The geometry was such that a beam particle would have to scatter in counter 3 in order to fulfill geometrical requirements. Although the momentum acceptance of the spectrometer extends beyond 100 MeV/c (the acceptance decreases slowly, limited by the chamber apertures), the number of events above 60 MeV/c was only 5×10^{-5} times the number of μ-e events. Since the traversing beam particles had momenta up to 100 MeV/c, this proves the above statement.

B. Field Homogeneity

Over most of the useful region of the spectrometer, the magnetic field is uniform to better than 0.05%. Some fraction of the lowest-energy electrons, however, passing near the coils, traverse during ~30% of their path fields up to 0.3% higher than the average. These higher fields bend more of such electrons into the virtual detector than would a uniform field. However, calculations show this bias to be negligible. Experimentally, we find that restricting the trajectories to regions of essentially uniform field (by smaller virtual detectors and/or smaller momentum bites) makes no significant change in ρ.

IV. ANALYSIS

Before making a direct comparison of the theoretical and experimental spectra, it is of course necessary to fold the momentum resolution of the spectrometer into the assumed theoretical spectrum. This resolution is governed (a) by collisional and radiative energy losses in the source counter, (b) by multiple scattering in material between the first and last wire chambers, and (c) by the spatial resolution of the wire chambers. Effects (b) and (c) together determine the "internal" resolution of the spectrometer, i.e., the momentum resolution for monoenergetic electrons incident on the first wire chamber. The resolution function is discussed in detail in Appendix C.

A. Statistical Analysis

A least-squares fit for ρ and η was made by folding the resolution function into the theoretical spectrum of Eq. (7) using a mesh size of 0.002, and computing χ^2 for various values of ρ and η. The results of this calculation for the 1734-G data and for the 1300-G data are shown in Fig. 6, where we display curves of constant χ^2 as functions of ρ and η. The points for which $\chi^2=\chi_{\min}^2+1$

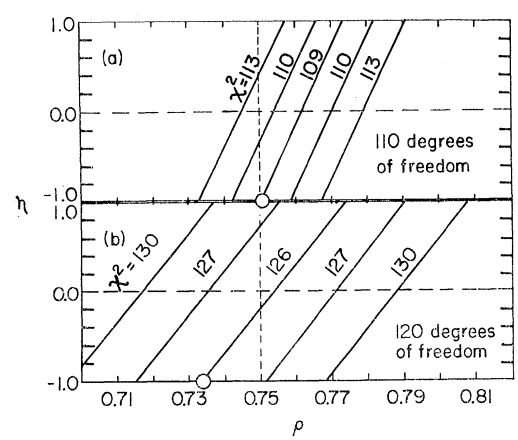

FIG. 6. Curves of constant χ^2 versus ρ and η; these are portions of ellipses, approximated here by straight lines. The circles are the absolute minima of χ^2 attained with the constraint $|\eta|<1$. (a) 1734-G data; (b) 1300-G data.

represent one standard deviation away from the best fit, and the locus of these points is an elongated ellipse extending far outside the region $|\eta| \leqslant 1$.

If the normalization of the 1300-G data relative to the 1734-G data were known, the statistical error would be reduced appreciably by appropriately fitting a theoretical spectrum to both sets of data simultaneously. However, to derive any benefit from this procedure, the relative normalization must be known to an accuracy of $\sim 10^{-3}$, which because of systematic effects is a practical impossibility. If this relative normalization is not known, then it *must* be treated as an *additional* free parameter in the fitting procedure; the correlation between it and ρ is such that the error in ρ is simply that obtained from averaging the results of separate fits, as is done here.

The information contained in Fig. 6 may be expressed fruitfully in three ways: (1) To compare with previous experiments, we may constrain η to $\eta=0$; then the variation of χ^2 with ρ along the line $\eta=0$ gives the results of a one-parameter fit for ρ. This procedure has no physical significance other than furnishing one form of a consistency check with the $V-A$ theory, a check which is more logically performed by (2) constraining ρ to $\rho=\frac{3}{4}$ (the two-component neutrino hypothesis) and noting that value of η, along the line $\rho=\frac{3}{4}$, which minimizes χ^2. This then constitutes a one-parameter fit for η. (3) We may leave *both* ρ and η free, subject to the constraint $|\eta|<1$. In this case the statistics are such that η is essentially undetermined and the error in ρ is partly statistical and partly due to the constraint on η. A reasonable way of stating the result is the following: for η constrained to $\eta=-1$, $\rho=\rho_{+1}\pm\sigma_0$. Then, for any η ($|\eta|<1$), we say that ρ lies in the interval $(\rho_{-1}-\sigma_0)<\rho<(\rho_{+1}+\sigma_0)$, with the best estimate of ρ given by the point where χ^2 is minimum, which is not necessarily at the center of this interval.

The results expressed according to these three viewpoints are summarized in Table II, where the errors quoted include estimates of systematic errors. We defer discussion of the results until we have discussed the latter.

B. Estimate of Systematic Errors

The main source of systematic error in this experiment is the calibration of the momentum scale. At 1734-G, $x=1$ corresponds to a radius of 100 cm; shifting the spectrum to coincide with the theoretical edge calibrates the spectrometer for trajectories with 100-cm radius. Unfortunately we do not have a spectrum taken at a higher field, which would provide a calibration of trajectories of smaller radius. As it is the trajectories of 100-cm radius which have the smallest sagittae provide the most stringent check on the absolute location of the wire chambers. As noted above, their momenta were low by 0.003; the trajectories of smaller radius, which have sagittae up to twice as large, could have momenta low by $\sim$0.001 to 0.003. This uncertainty in the stretching of the momentum scale introduces an uncertainty into the best estimate of ρ (for $\eta=0$) of $_{-0.003}{}^{+0.000}$.

TABLE II. Experimental results.

Magnetic field	1300 G	1734 G	
Momentum region[a]	0.52 −0.76	0.70 −0.92	Weighted average
Number of events	80×10^3	200×10^3	280×10^3
$\eta=0$; $\rho=$	0.754 ± 0.020	0.762 ± 0.010	0.760 ± 0.009
$\rho=\frac{3}{4}$; $\eta=$	-0.2 ± 1.0	-1.0 ± 0.8	-0.7 ± 0.6
$\lvert\eta\rvert<1$; $\rho=$	$0.733_{-0.020}{}^{+0.060}$	$0.750_{-0.010}{}^{+0.030}$	$0.765_{-0.028}{}^{+0.015}$

[a] In natural momentum units (52.83 MeV/c = 1).

Neglect of external radiative losses in the source would lower ρ by 0.008. The theoretical bremsstrahlung spectrum for carbon is probably accurate to within a few percent. The mean radiative path in the source depends on the distribution in depth of the decays, which is known only to the extent that we observe that electrons leaving the source produce scintillator pulses which vary over a range of approximately eight to one. In making the bremsstrahlung correction, we took for the radiative path one-half the total thickness, which could underestimate the effect by as much as 10%; hence this introduces an uncertainty into the best estimate of ρ of $_{-0.000}{}^{+0.001}$.

The experimental spectrum is essentially zero for momenta 0.07 greater than the endpoint, which is at 0.992. Hence the upper limit of the region of fit was taken as 0.92, i.e., approximately 0.07 less than the endpoint. Varying this upper limit in the region from 0.90 to 0.92, we obtained consistent values of ρ and χ^2. If we include data above 0.92, χ^2 increases steadily and ρ decreases; this presumably reflects the uncertainties in the resolution function discussed in Appendix C. Varying the lower limit of the region fit from 0.70 to 0.74 also produced consistent values of ρ and χ^2. The stability of ρ and of χ^2 over various regions of the spectrum constitutes a check of several possible systematic effects, which are independently estimated to be negligible.

C. Discussion of Results

The final results of this experiment are summarized in Table II, where the errors quoted include estimates of systematic errors. The fits are excellent in terms of the χ^2 criterion: $\chi^2=109$ for 110 ± 15 expected (1734-G data), and $\chi^2=126$ for 120 ± 16 expected (1300-G data). The spectra are plotted in Fig. 7, and the deviations between the experimental points and the fit are shown in Fig. 8. The spectrum is given numerically in Table III, for a mesh size of 0.01. It is seen that the data are in agreement with the predictions of the $V-A$ theory ($\rho=\frac{3}{4}$, $\eta=0$). Considering that η is restricted to the range $|\eta|\leqslant1$, we may assign an unsymmetrical error estimate to η: $\eta=-0.7_{-0.3}{}^{+0.6}$.

To compare with other experimental results, we now consider the case in which we impose the constraint

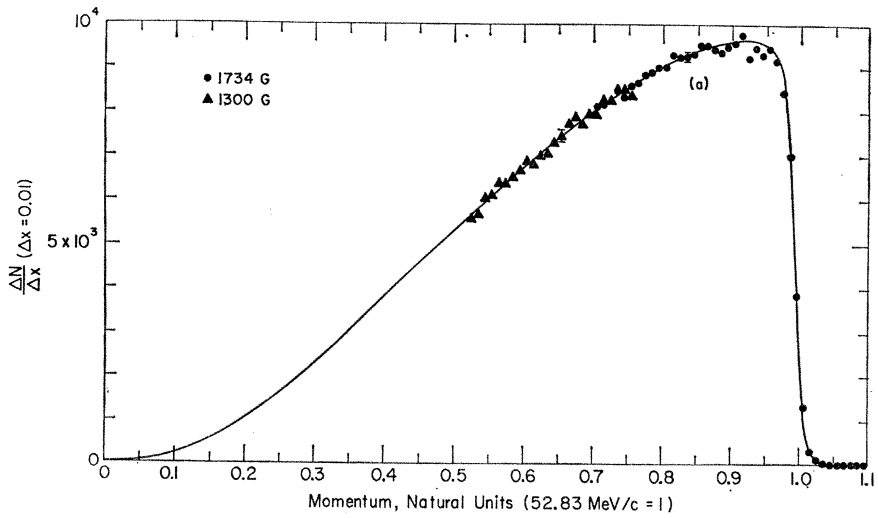

FIG. 7. Experimental points. The points taken at 1300 G have been multiplied by a factor of 2.19 for display. The solid line represents the Michel spectrum for $\rho=0.760$ and $\eta\equiv0$, inclusive of radiative corrections (Ref. 13), with allowance for source losses and finite resolution.

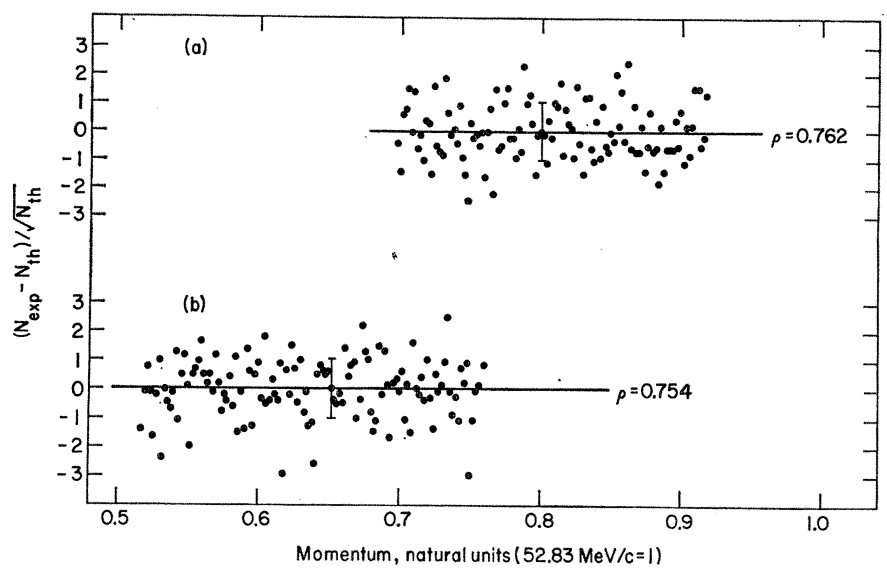

FIG. 8. Deviations of the experimental points from the best-fit theoretical curves, plotted in steps of 0.002 (natural momentum units). (a) 1734-G data; (b) 1300-G data.

$\eta=0$; this yields $\rho=0.760\pm0.009$.[36] This result contradicts several previous experiments[19,23,24]; in view of the vastly improved control over systematic effects in the present experiment, we are inclined to consider those results obsolete.

Of the two bubble-chamber experiments, Plano's[21] has four times more events. In fact, for the general case of η constrained only to $|\eta|\leqslant1$, his statistical power is comparable to ours, although he has only 3% as many events. This is due to the fact that by observing the entire spectrum the differences between the ρ- and η-associated functions in the theoretical spectrum become statistically apparent and the ρ-η correlation is greatly reduced. The interpretation of Plano's data as regards ρ and η is somewhat ambiguous due to an admitted deficiency of low-energy electrons,[28] but with the constraint $\eta=0$ his value of $\rho(0.780\pm0.025)$ is consistent with $V-A$. (It should be emphasized that, with the exception of the thesis of Peoples, the influence of η on the results of other experiments is not known.) The bubble-chamber experiment of Block *et al.*[22] yielded, for $\eta\equiv0$, $\rho=0.751\pm0.034$, in good agreement with $V-A$.

The experiment of Bardon *et al.*[17] utilizes a technique similar to ours. With the constraint $\eta=0$ they obtain $\rho=0.750\pm0.003$, and with the constraint $\rho=\frac{3}{4}$ they obtain $\eta=0.05\pm0.50$, again in agreement with $V-A$.

There is agreement with the result of Dudziak *et al.*[20]; from our experience, we are however inclined to believe that the error assigned in Ref. 20 is unrealistically small. Indeed, the backgrounds were large, and the resolution

[36] Our preliminary result (Ref. 1), based on a spectrum with 8×10^4 events, was $\rho=0.753\pm0.011$ (including a correction for external radiative losses, which were originally neglected.) These data are not included in our final ρ value, as a much larger body of data, of better quality, was collected after a slight adjustment of the spectrometer.

TABLE III. $\Delta N/\Delta x$ versus $\bar{x}$.

	0.005	0.015	0.025	0.035	0.045	0.055	0.065	0.075	0.085	0.095
					1300 G					
0.5	2361	2479	2556	2593	2758	2793	2918	2920	2966	3042
0.6	3146	3111	3290	3230	3351	3403	3552	3612	3526	3642
0.7	3638	3777	3780	3910	3896	3838				
					1734 G					
0.7	8135	8185	8266	8477	8331	8584	8646	8853	8917	9026
0.8	9028	9299	9259	9259	9319	9550	9542	9437	9371	9504
0.9	9581	9788	9241	9478	9307	9458	8987	8434	7027	3880
1.0	1316	301	123	50	15	10	3	3	0	0

function—which is of great importance in a point-by-point measurement—was inferred almost entirely on theoretical grounds. The magnetic-spectrometer experiment of Kruger[18] utilized thick sources, necessitating rather large corrections; however, high accuracy was not claimed ($\rho=0.774\pm0.042$).

In conclusion, of the four most accurate and reliable measurements of ρ (Plano,[21] Block *et al.*,[22] Bardon *et al.*,[17] and this experiment), all agree with the predictions of $V-A$ theory ($\eta=0$ and $\rho=\frac{3}{4}$).

ACKNOWLEDGMENTS

I wish to thank Professor V. L. Telegdi for suggesting this problem and for his guidance, encouragement, and wholehearted participation in the preparation, performance, and analysis of the experiment. I also thank him for his inspired teaching of fundamental physical principles.

I thank my collaborators, Richard Ehrlich, David Fryberger, Richard Powers, and Jurgen Bounin, for contributing many months of great physical and intellectual effort. To David Fryberger I am also indebted for important contributions to the design and execution of the experiment, and for valuable discussions. Tom Nunamaker contributed much, both in circuit design and in spark-chamber construction. I thank Ronald Swanson for initiative and attention to detail in technical matters, and Karel Sebesta for careful electrical and mechanical constructions. I wish to acknowledge useful discussions with Professor R. H. Hildebrand.

This experiment owes its inception to the invention of the wire spark chamber by Michael Neumann at the Institute for Computer Research (ICR). To him, and to the director of ICR, Professor R. H. Miller, I am indebted for enthusiastic support. I express my heartfelt gratitude to the many members of ICR who made personal sacrifices to ensure our success; particular thanks go to Charles Robinson and to Miss Evi Mayer.

APPENDIX A: SPECTROMETER DESIGN AND CONSTRUCTION

A. Initial Design Criteria

In this section we list and discuss the criteria for the design of a spectrometer (utilizing counters and spark chambers) suitable for the experimental goals described in Sec. I.

1. Wide Momentum Acceptance

It is desirable to include, at a given magnetic field setting, a wide momentum range, and to determine ρ from the spectral shape in that range alone. (ρ is then determined essentially by the slope of the spectrum.) This is to eliminate systematic normalization errors associated with the difficulty of measuring reliably pion or muon stopping rates, and is in contrast to classical magnetic-spectrometer techniques in which the spectrum is measured point by point. Within the momentum range selected, the acceptance as a function of momentum must be uniform (or known).

2. Homogeneous Spectrometer Field

Data analysis and control over systematic effects in the momentum acceptance and momentum scale are greatly simplified by the use of a homogeneous magnetic field. With muon decay taking place within such a field the entire electron trajectory is a helix.

3. Capability to Measure the Anisotropic Spectrum

We imposed the requirement that it be possible to measure the asymmetry parameter δ subsequently in essentially the same apparatus. With the source in the spectrometer field, this criterion restricts the field strength to be low enough to permit one to time the muon precession. In order to determine the phase of the muon spin (for any decay-electron momentum) it is necessary to subdivide the angular distribution into more than the minimum "backward" and "forward" hemispheres. Subdivision into four equal quadrants of 10 nsec each is practical in a field of 1850 G with existing electronics.

We therefore imposed the condition that even in the measurement of the isotropic spectrum (averaged over angles) the magnetic field not exceed 1850 G; since the momentum resolution deteriorates with decreasing field, this maximum field was chosen as the approximate design value. (The highest field setting actually used in the experiment was 1734 G.)

4. Momentum Resolution

For ρ in the neighborhood of $\frac{3}{4}$, the theoretical spectrum varies slowly with momentum, except for the discontinuity at $x=1$. Therefore, folding in a symmetric resolution function changes the spectral shape only near the discontinuity; if this region is excluded in a fit for ρ, the value of ρ obtained is insensitive to uncertainties in the resolution function. On the other hand, straggling and bremsstrahlung in the source contribute low-energy tails to the resolution function which change the slope of the spectrum and, hence, the apparent value of ρ. Therefore the stopping material must be kept as thin

as possible to minimize systematic errors arising from uncertainties in the radiative energy-loss distribution.

There are, however, limits to how thin the source may be. For measuring the isotropic part of the spectrum, stopping pions provide a convenient sample of unpolarized muons, but most of these muons will escape if the source is thinner than their range (0.25 g/cm^2). Certain kinds of background are minimized by localizing the electron's parent muon, so that muon escape is undesirable. Furthermore, in practice, available stopping-pion and muon fluxes also set practical limits on the source thickness. On the basis of these considerations, we decided to stop pions in a 0.3-g/cm^2 ($\frac{1}{8}$-in.) scintillator.

5. *Absolute Momentum Scale*

Determination of the electron end-point momentum (as a measurement of the μ-neutrino mass) was not a goal of this experiment; however, the absolute-momentum scale must be known rather well because ρ is somewhat sensitive to systematic errors in the momentum scale. For example, fitting over the region $0.72 \leqslant x \leqslant 0.92$, shifting the momentum scale by $\Delta x = 0.006$ produces a change in ρ of 0.01. On the other hand, the end point W is extremely insensitive to a (possibly) nonzero μ-neutrino mass λ $[W = (\mu^2 + m^2 - \lambda^2)/2\mu]$, and hence the observed end point (corrected for source losses) may be used to calibrate the spectrometer sufficiently accurately. Moreover, the end point is also sufficiently insensitive for our purposes to moderate changes in ρ.

B. Realization

Figure 1 shows the final layout of the spectrometer. The magnet used[37] is of the current-sheet type, and has a large useful volume ($2\times2\times8$ ft^3) in which the field is very uniform ($<0.05\%$ without shimming). The original slot in the coils through which pions could be injected into the magnet appeared too small for our purposes. We remedied this by replacing several layers of the original coils with new, lighter coils whose thickness is less than the pion range (for a 150-MeV/c beam), and pions are injected *through* these new coils. Vertical shims beside the coils compensated for slight geometrical differences in the two types of coils. After shimming, the field homogeneity was found to be better than 0.05% except within 3 in. of the coils, where some of the lowest-momentum particles traverse an inhomogeneity of $\sim$0.3% over $\sim$30% of their path.

At a field of 1700 G the radius of curvature of a 50-MeV/c ($x=1$) electron is 100 cm. The magnet dimensions are too small to permit the use of 180° focusing geometry[17] at this field, and the geometry is of a nonfocusing type.

Pions which come to rest in counter 3 ($\frac{1}{8}$-in. plastic scintillator) yield muons most of which also stop in counter 3. Electrons from their decay traverse scintillation counters 3, 4, and 5 and fire wire spark chambers $R1$, $R2$, $R3$, $R4$ which measure the radius of the helix, and $P1$, $P2$, $P3$ which measure the pitch. Since both the horizontal (circular) projection and the slope of the helix are thus overdetermined, it is possible to eliminate events in which the electron followed an irregular trajectory (scattering off the walls, etc.). Helium-filled boxes with $\frac{1}{2}$-mil Mylar windows are placed between spark chambers to reduce multiple scattering of the electrons. Chambers $R3$ and $P2$, and to a lesser extent $R2$, restrict the momenta accepted with good efficiency to those corresponding to radii of curvature in the range $70 \leqslant r \leqslant 110$ cm.

The high-momentum trajectories have the smallest sagittae; a circle of 100-cm radius has a sagitta of $\sim$5 cm. With our spark chambers (yielding ±0.03 cm in spatial resolution) a momentum resolution $\Delta p/p = \pm0.6\%$ is expected due to spatial resolution alone. This $\Delta p/p$ is comparable to the momentum smearing produced by the distribution in depth of the muon decays within the source, if the latter is $\sim$0.3 gm/cm^2 thick. Allowing for the effects of multiple scattering, one anticipates an over-all momentum resolution of $\sim\pm1\%$.

The entire assembly, with cables for pulsing and reading the chambers and tubing for supplying them with neon, is mounted on a false floor. After measuring the chamber positions on a milling machine, the entire assembly is lowered into the magnet. The scintillation counters are supported by the magnet roof and are separate from the wire-chamber assembly.

APPENDIX B: WIRE SPARK CHAMBERS

A. Chamber Construction and Readout

Wire spark chambers with magnetic-core readout[2] differ from ordinary visual spark chambers in that one of the plane electrodes (the "write plane") is divided into wires each of which is grounded through a ferrite core. When a spark strikes a write wire, current flows through the core and "sets" it, thus digitizing the spark location. This information may then be transmitted conveniently to a computer or stored on magnetic tape.

The wire spark chambers used in this experiment consist of 0.25-in. (6-mm) glass "picture frames" wound on both sides with 4-mil (0.1-mm) duraluminum wire spaced 24 to the inch ($\sim$1-mm spacing). Most chambers have 256 wires on each side and are 35×35 cm^2 overall, with 25×25-cm^2 active areas. Because glass has a rather high dielectric constant, the capacitance of a chamber is typically 350 pF; this could be reduced through more careful placement of the electrical connections. The chambers were covered with 0.5-mil Mylar and a Ne-He mixture (9:1) flowed through them during operation. If the wires are considered spread out to form a continuous sheet, then each chamber has a

[37] We are indebted to Professor S. C. Wright for the loan of this magnet.

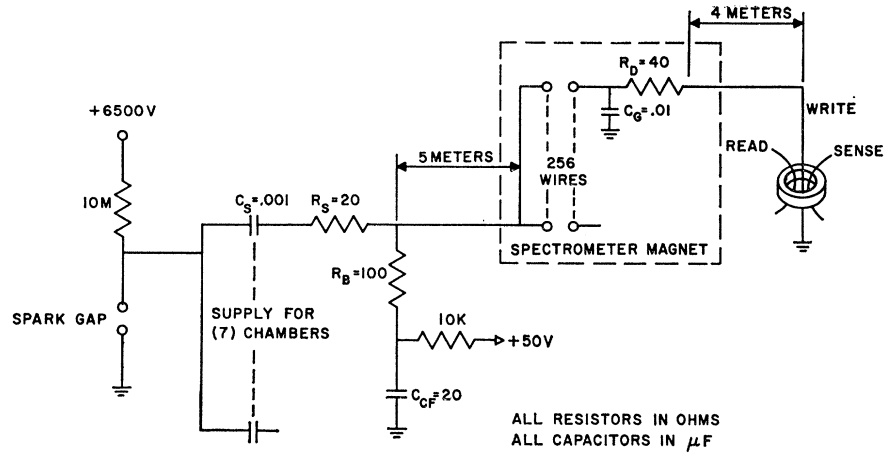

FIG. 9. Electrical connections to the wire spark chambers.

mass thickness of 5.6 mg/cm^2 and is equivalent to 2×10^{-4} radiation lengths.

The wire spacing was kept uniform by winding the frames on a drum which turned on a machine screw of 24 turns per inch. After winding of one side was completed, the wires were glued to the glass with epoxy. Then the wires were cut and trimmed and the other side was wound to make two planes of parallel wires. One set of wires was tied to a common bus and used as the high-voltage ("pulse") electrode; the other set was crimped to connectors glued to the glass frame. Plug-in cables[38] made the connection between the wire chamber and a memory plane of ferrite cores. Two chambers are needed to obtain both x and y coordinates.

Each ferrite core is threaded not only by a "write" line but also by "read" and "sense" lines. The readout system[39] sends a reset pulse down a read line through 32 cores. In those cores which were "set" by spark current, the read current induces a response in the sense line sufficient to set a flip-flop in a 32-bit register. If no flip-flops are set, the readout system proceeds immediately to interrogate the next group of 32 cores. When a nonempty group is found, all 32 bits are transmitted (to a computer or other storage medium) together with an 8-bit address and 8 dummy bits, making a 48-bit word. After all memory planes have been read out, an additional 48-bit word is transmitted, containing other information such as counter logic results, etc.

B. Chamber Performance

The core planes had to be located outside the spectrometer magnet. For this reason, the electrical connections to the chambers were somewhat unconventional; we shall first discuss these with reference to Fig. 9. Each wire of the write plane is ac-grounded by a capacitor C_G, eliminating erratic behavior due to the large inductance of the long cables (4 m) leading to the core planes. To keep neighboring wires at equal potentials, these capacitors C_G must all be the same distance from the write-plane wires. Resistor R_0 damps oscillations which would otherwise tend to reset the core.

The spark-gap pulser[40] is supplied with +6.5 kV, resulting in a negative pulse of ~4 kV on the chamber. The series resistor R_S and bleeder resistor R_B (grounded through the clearing-field capacitor C_{CF}) are close to the supply capacitor C_S, and there is a 5-m cable (RG-59U) between these elements (which are outside the spectrometer magnet) and the chamber. With this arrangement one can easily adjust the bleeder resistors in order to optimize chamber performance as described below.

The chambers were carefully tested prior to the experiment, with special emphasis on efficiency and spatial resolution. For most of the test three chambers were used at a time; these were equidistant and carefully aligned parallel to each other. This setup was traversed by a meson beam (150 MeV/c), and triggered by a coincidence between scintillators placed upstream and downstream. Data were analyzed on line by MANIAC III, a technique permitting the fastest possible feedback after trial modifications of running conditions. The computer first found (a) the number of adjacent wires struck by a spark (called the "spread," n) and (b) their centroid, which is identified as the horizontal trajectory coordinate. One and only one spark (with $n>1$ in general) in both of the outer chambers defined a particle trajectory, in which case the middle chamber was examined and the event classified into one of four categories: (a) "good"—one and only one spark in the middle chamber, and it being within 5 mm of the position predicted by the outer chambers; (b) "spurious"—one or more additional sparks elsewhere in the middle chamber; (c) "misplaced"—only one spark, and it being more than 5 mm from the predicted position; (d) "miss." The percentage of misplaced events is generally to be divided by three, since any of the three chambers

[38] "Spectra-Strip," Spectra-Strip Wire and Cable Corporation, Garden Grove, California.

[39] The readout system was designed by J. Bounin and R. H. Miller and is built of DEC System Modules.

[40] L. Lavoie, S. Parker, C. Rey, and D. M. Schwartz, Rev. Sci. Instr. 35, 1567 (1964).

could be at fault. (These "misplaced" events were not merely the tail of the resolution curve. Their number exhibited no rate dependence and is consistent with π-μ decay in flight; nevertheless, as this hypothesis was not explicitly tested, we here attribute these events to the chamber performance.) With this correction, it was found that typical performance was characterized by: good events—96.1%; spurious events—2.8%; misplaced events—0.9%; missed events—0.2%, over a supply high-voltage range of 6.5–7.0 kV. Moreover, the efficiency was uniform (to a statistical accuracy of 1.5%) over the whole chamber.

We determined the distribution of the differences between the observed spark centroids in the middle chamber and the predicted positions. Conditions were such that multiple scattering was negligible and the spatial resolution was determined solely by spark jitter. Under normal conditions the observed distributions were essentially Gaussian with a standard deviation $\sigma'=0.39$ mm. Assuming the resolution to be the same in all three equidistant chambers, this implies that their intrinsic resolution is

$$\sigma=\sigma'/\sqrt{\tfrac{3}{2}}=0.32\pm0.02\text{ mm}.$$

This resolution was achieved when each chamber had an average spark spread $\bar{n}$ of approximately 2.5 wires (equal numbers of sparks with $n=2$ and $n=3$), a situation that ensures high efficiency and Gaussian spatial resolution.[41] It was found that $\bar{n}$ is quite sensitive to electrical and gas conditions and thus provides an excellent monitor thereof. Normally all chambers were pulsed from the same gap, and the individual bleeder resistors R_B were adjusted to make each chamber have $\bar{n}=2.5$ wires.

The pulse plane is pulsed negative, and since the (negative) electrons in the ion trail initiate the spark, the x coordinate given by the write plane is in general to be correlated with a z coordinate (perpendicular to the plane) somewhere between the pulse and write planes. In order to study possible systematic spatial displacements for particle trajectories at non-normal incidence, a fourth chamber was placed next to the middle chamber. The original three chambers all had the same orientation of pulse and write planes, while the fourth was turned through 180°. Thus the systematic displacements were all, in the same sense, in the original three chambers, but, in the opposite sense, in the fourth chamber. To eliminate shifts due to non-normal incidence in the absence of a clearing field, it was found sufficient to consider that the write plane was not in its true location but midway between the physical pulse and write planes. With this correction applied, the addition of a clearing field of a polarity opposite to the high-voltage pulse was found to shift the spark centroid (up to incident angles of 20°) by 0.001 mm per degree of incident angle and per volt of applied clearing field. During the experiment we operated with a clearing field of 50 V, and the maximum incident angle on any plane was 20°; hence the largest correction to be made was 1.0 mm. For a given clearing-field voltage one can choose an effective write-plane z coordinate which will compensate for the clearing-field shifts.

[41] For a discussion of how the average spread influences the resolution, see Ref. 1.

APPENDIX C: THE RESOLUTION FUNCTION

The experimental energy-loss distribution for 15.7-MeV electrons (e^-) of Goldwasser *et al.*,[42] which includes, except for a low-energy tail, both collisional and radiative losses, was summed over the thickness of the source counter. The average energy loss was checked by placing an identical scintillator with wrappings between the source counter and the first wire chamber, and noting the displacement of the spectrum edge. The low-energy tail from ionization was extended according to the E^{-2} dependence derived by Landau.

Radiative losses of more than 5 MeV were allowed for by folding in the bremsstrahlung spectrum of Bethe and Heitler.[43] As the screening has been computed on the basis of the Thomas-Fermi atom, there could be some question as to whether this spectrum is correct for a low-Z element such as carbon. However, Wheeler and Lamb have shown[44] that exact calculations for hydrogen, and Hartree self-consistent field calculations for nitrogen, are in agreement with calculations based on the Thomas-Fermi atom. Hence it is reasonable to suppose that for $Z=6$ the Bethe-Heitler spectrum should be quite accurate. The thickness of the source counter and wrappings was 0.45 g/cm^2 or 0.01 radiation lengths, and we took half of this (0.005) for the radiative thickness t. The distribution of energy loss k for an electron of initial energy E_0 was taken to be $1.35\ t(1-k/E_0)\Delta k/k$, which is an adequate representation of the Bethe-Heitler spectrum for the relevant range of K and E_0.

The internal resolution was determined from the experimental data themselves, using the radial and pitch deviation distributions Δ_4 and Δ_z shown in Fig. 5. If all four points in $R1$, $R2$, $R3$, $R4$ lie on a circle, Δ_4 is of course zero. The geometry is such that a radial displacement of the trajectory (essentially perpendicular to the trajectory) of 1 mm in $R1$ produces $\Delta_4=1$ mm, as does a 1-mm displacement in $R4$. A displacement of 1 mm in $R2$ or $R3$ produces $\Delta_4=2.5$ mm. Let d_i= the deviation in the ith wire chamber due to multiple scattering and spark jitter, and neglect multiple scattering in the material (He) between the chambers. Then

$$\Delta_4=-d_1+2.5d_2-2.5d_3+d_4. \tag{9}$$

[42] E. L. Goldwasser, F. E. Mills, and A. O. Hanson, Phys. Rev. **88**, 1137 (1952).

[43] B. Rossi, *High-Energy Particles* (Prentice-Hall, Inc., Englewood Cliffs, New Jersey, 1952).

[44] J. A. Wheeler and W. Lamb, Phys. Rev. **55**, 858 (1939).

The electron scatters in chamber $R2$ through an angle θ_2 (in the plane) and in chamber $R3$ through an angle θ_3. Let s_i be the spark jitter in the ith wire chamber, and c be the chord length between $R2$ and $R3$, and between $R3$ and $R4$.

Assume that an electron starts from midway between $R2$ and $R3$ and proceeds both left and right. This mathematical trick allows one to write

$$\begin{aligned} d_1&=s_1+c\theta_2,\\ d_2&=s_2,\\ d_3&=s_3,\\ d_4&=s_4+c\theta_3,\\ \Delta_4&=(s_4-s_1)+2.5(s_2-s_3)+c(\theta_3-\theta_2). \end{aligned} \tag{10}$$

$\langle\Delta_4^2\rangle_{\text{av}}=14.5\langle s^2\rangle_{\text{av}}+3c^2\langle\theta_2^2\rangle_{\text{av}}$ since the spatial resolution of each chamber is the same and since $\theta_3^2=2\theta_2^2$ because of the presence of two wire chambers $R3$ and $P2$ as opposed to one, $R2$.

Similarly,

$$\Delta_z=s_{p3}+0.5(s_{p1}-s_{p2})+c(\Phi_{p3}-0.5\Phi_{p2}) \tag{11}$$

and

$$\langle\Delta_z^2\rangle_{\text{av}}=1.5\langle s^2\rangle_{\text{av}}+2.25c^2\langle\theta_2^2\rangle_{\text{av}}.$$

Since $\langle\Delta_4^2\rangle_{\text{av}}$ and $\langle\Delta_z^2\rangle_{\text{av}}$ are known experimentally, $\langle s^2\rangle_{\text{av}}$ and $\langle\theta_2^2\rangle_{\text{av}}$ can be determined. Moreover, the spatial resolution $\langle s^2\rangle_{\text{av}}$ for these wire chambers was established by careful studies performed outside the magnet, yielding $\langle s^2\rangle_{\text{av}}^{\frac{1}{2}}=0.32$ mm. Therefore $\langle\theta_2^2\rangle_{\text{av}}$ is overdetermined, and we find Eqs. (10) and (11) consistent with $(\theta_2^2)^{1/2}=3.2\times10^{-3}$ rad at $p=48$ MeV/c. Note that $\langle\Delta_z^2\rangle_{\text{av}}$ is essentially determined by scattering alone, whereas $\langle\Delta_4^2\rangle_{\text{av}}$ is due approximately equally to scattering and to spark jitter. For geometrically similar orbits at a lower field (1300 G) we find $(\theta_2^2)^{1/2}=4.3\times10^{-3}$ rad at $p=36$ MeV/c, verifying that $(\theta_2^2)^{1/2}$ is inversely proportional to the momentum. Because the Δ_4 and Δ_z distributions had non-Gaussian wings, we took for their standard deviations their half-widths at half maximum divided by 1.17.

Next, the Δ_4 and Δ_z distributions were reproduced by a Monte Carlo program, whose inputs were Gaussian spatial resolution and scattering distributions for monoenergetic electrons, of widths determined above. The program also produced Gaussian Δ_p' and response distributions. The $\Delta p'$ distribution had the experimental width. The response function determined in this way is assumed to be essentially correct in width but not necessarily in shape. The *ratio* of the full widths at half-maximum of the computed (Monte Carlo) response function and Δ_4 distribution was used to scale up the experimental Δ_4 distribution to give the presumed "true" response function. This approach should insure that the derived response function not be sensitive to uncertainties in this partly theoretical treatment. The "true" response function was determined in this manner as a function of momentum in the range of interest.

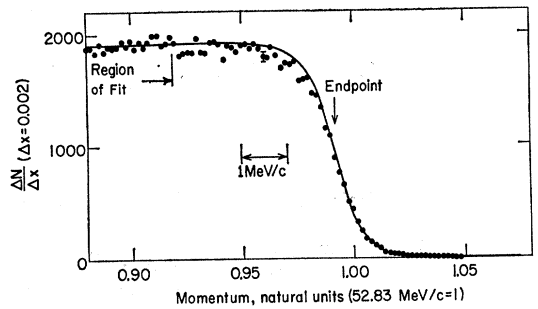

FIG. 10. Experimental spectrum in the neighborhood $x=1$; the mesh size is 0.002. The curve is the result of fitting the data in the interval $0.70<x<0.92$ to the theoretical spectrum, after folding in the experimental resolution. The small systematic deviations from this curve are ascribed to uncertainties in the resolution function.

As discussed in Appendix A, for $\rho=\frac{3}{4}$ the experimental resolution alters the spectrum only in the neighborhood of $x=1$; hence the resolution appropriate to $x=1$ was folded into the theoretical spectrum, ignoring the momentum dependence of the resolution. Including both target loss and the intrinsic resolution, the resolution function had a full width at half-maximem of 0.020 ($=1$ MeV/c).

In addition to energy loss in the source there are two effects which shift the momentum scale: (a) Energy loss in the spark chambers and helium (between the source and the final chamber) produces a shift downward of $\Delta x=0.0015$, as determined by a ray-tracing program.[45] (b) Spark shifts due to the applied clearing field as discussed in Appendix B on the average shift momentum down by $\Delta x=0.0015$. When these corrections are applied we find that the experimental end point is low by $\Delta x=0.003$, which we attribute to measurement uncertainties in the location of the spark-chamber wires. These locations were measured to approximately ±0.08 mm (±0.003 in.); for typical sagittae of ~50 mm, this introduces a momentum error of approximately ±0.002. As discussed in Appendix A, we use the end point as a momentum calibration and shift the data to coincide with the folded theoretical spectrum (for $\rho=\frac{3}{4}$) as shown in Fig. 10, where it is seen that the shape of the experimental spectrum agrees fairly well with the resolution function derived above. However, just above $x=1$ the experimental points lie slightly above the folded theoretical spectrum, and just below $x=1$ they lie slightly below the theoretical spectrum. This indicates that the width of the true experimental resolution function is relatively a few percent wider than the calculated width, a possibility we cannot exclude, considering the way in which it was derived. We therefore attach no special significance to these deviations.

[45] We are indebted to Lloyd Hyman and David Gold of Argonne National Laboratory for this program (TRACK).